Characterization of the Reaction Products of Laser-Ablated Early Lanthanide Metal Atoms with Dinitrogen. Infrared Spectra of LnN, LnN_2, $(LnN)_2$, and $Ln(NN)_x$ Molecules

Stephen P. Willson and Lester Andrews*

Chemistry Department, University of Virginia, Charlottesville, Virginia 22901

Received: July 31, 1998; In Final Form: October 6, 1998

This paper summarizes the first part of a systematic study of the small nitride molecules and simple dinitrogen complexes of the lanthanide metals except promethium. Simple nitrides of the general formulas LnN and $(LnN)_2$ have been identified for Ln = Ce, Pr, Nd, Sm, Eu, and Gd; LnN_2 has been identified for Ln = Ce, Pr, Nd, and Sm. Several dinitrogen complexes of the type $Ln(N_2)$, Ln(NN), $Ln(NN)_2$, and $Ln(NN)_x$ have also been observed in matrix infrared investigations. The tendency of the identified nitrides to complex dinitrogen is readily determined from experimental data, which provide frequencies for observed fundamentals both before and after dinitrogen complexation. Several reaction pathways to formation of the small nitrides have been explored. The favored pathway to the $(LnN)_2$ molecule involves reduction of N_2 by two Ln metal atoms concurrent with complete scission of the N≡N triple bond.

Introduction

Of the lanthanide mononitrides, CeN alone has been previously observed but only in gas-phase mass spectrometric work.[1] Because gas-phase frequencies of the lanthanide mononitrides have not been reported, the assumption is made that they relate to the matrix-isolated mononitrides in parallel fashion to the transition metal mononitrides, several of which have been reported both in gas-phase and matrix isolation studies. Examples from each transition metal row include the vibrational fundamentals of TiN, MoN, and ReN, which are known to ±0.1 cm^{-1} accuracy from gas-phase spectra.[2−4] Recent matrix isolation work provides similar results, with frequencies red-shifted from the gas-phase values by 7.2, 5.8, and 4.5 cm^{-1}, respectively.[5−7] Although the fundamentals of additional transition metal mononitrides have also been determined by the matrix isolation technique, most have not yet been determined in the gas phase to allow similar comparison.[8−14] Because transition metal mononitride vibrational fundamentals from the first to the third row agree (±10 cm^{-1}) with the gas-phase data, it is reasonable to expect that the fundamentals of lanthanide mononitrides isolated in argon and nitrogen matrices and reported in this paper will be predictors of the gas-phase values. Frequencies observed in argon matrices are expected to be about 10 cm^{-1} lower than those in the gas phase, while fundamentals observed in nitrogen films are likely to be 50−80 cm^{-1} red-shifted from the gas phase because of ligation by dinitrogen.

Theoretical lanthanide work has concentrated on the small molecular systems for which experimental vibrational frequencies are largely absent.[15−18] No vibrational frequencies of the mono and dinitrides of the lanthanide elements have been reported in the gas phase. The current study reports the first experimentally measured vibrational frequencies of several lanthanide mono- and dinitrides as well as the dimers of the mononitrides in both solid nitrogen and argon matrices. In addition, N_2 vibrational frequencies of trapped complexes of the metals and metal nitrides are also provided.

In an ongoing search for improved catalytic conversion of N_2 to NH_3, recent inorganic studies in solution phases have discovered several examples of planar, side-on bonding of two metals to N_2 since the first such X-ray crystal structure by Evans et al.[19−21] In this laboratory, side-on bridging N_2 complexes in argon have been isolated without additional ligands and characterized by infrared spectroscopy. Several examples are presented in this and other publications from our laboratory, which demonstrate the ability of transition metal atoms to completely reduce the N_2 triple bond, forming rhombic metal nitride species; theoretical calculations show no remaining N−N bonding character after ring formation.[11−14]

Experimental Section

Lanthanide atoms supplied by laser vaporization of a metal target were reacted with molecular nitrogen in both argon and nitrogen matrices using techniques described in previous publications.[9,10,22,23] Experiments carried out in solid nitrogen films required sample deposition periods of 15−25 min; in argon, with N_2 concentrations ranging from 2 to 4%, about 1 h was required. Both types of experiments worked well with deposition rates of about 5 mmol/h onto a CsI window held at 6−7 or 10−11 K. Infrared spectra were recorded at 0.5 cm^{-1} resolution with a Nicolet 750 or a Nicolet 550 spectrometer after deposition and after each annealing or photolysis. The metal targets Ce (99.99%), Pr, Nd, Sm, Eu, Gd (all Johnson-Matthey 99.9%) were ablated with the 1064 nm fundamental of a YAG laser using 35−50 mJ pulses. For some experiments, isotopically scrambled N_2 was created by flowing the gas mixture through a microwave discharge (30 W) in a 6 mm o.d. quartz tube. Following deposition, argon matrices were annealed to 28 K and nitrogen matrices to 25 K. Then they were subjected to UV photolysis using a 175 W mercury street lamp (Philips H39 KB) without the globe (240−580 nm). An annealing cycle consists of raising the matrix temperature to the specified value, then lowering back to a deposition temperature of 6−7 or 10−11 K. Two or three additional annealings were then done, not exceeding 45 K for argon matrices or 35 K for nitrogen films, and additional spectra were recorded.

Results

The absorptions observed in all six of these metal nitride systems can be divided into three general regions of the infrared

10.1021/jp9832342 CCC: $15.00
Published on Web 11/14/1998

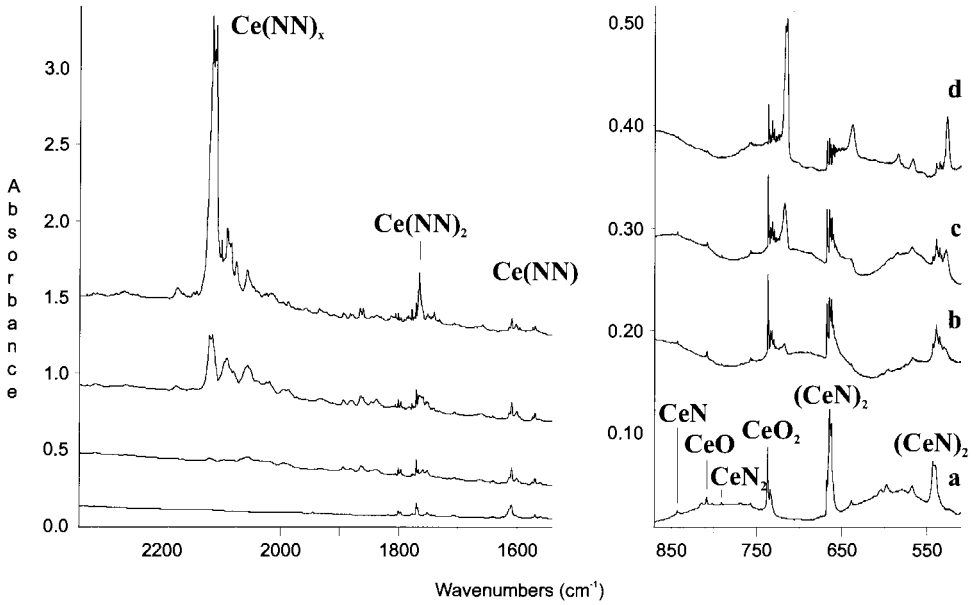

Figure 1. Infrared spectra in the 2340−1540 and 870−510 cm^{-1} regions for laser-ablated cerium atoms co-deposited with 2% $^{14}N_2$ in argon: (a) after 45 min deposition at 6−7 K; (b) after annealing to 20 K; (c) after annealing to 25 K; (d) after annealing to 35 K.

spectrum. There are several products that absorb in the traditional metal nitride stretching region between 450 and 1000 cm^{-1}, four of which show nitrogen $^{14}N/^{15}N$ ratios appropriate for Ln−N stretching modes. Absorptions that occur from 1200 to 2400 cm^{-1} are in the expected region for N_2 complexes and show the appropriate $^{14}N/^{15}N$ ratios for N−N stretching frequencies (Figure 1). In general, these bands increase on annealing but are not significantly affected by photolysis. In addition, absorptions observed in nitrogen films near 3400 cm^{-1} are in the region expected for overtones of dinitrogen complexes. Observed product peaks are fully delineated in Tables 1−6. Results of successive annealing cycles are included in the tables; photolysis data are also included when it provides useful information. Where matrix sites are present, only the primary peak is considered in the text, although significant sites are included in the tables. Representative spectra illustrated for Ce, Pr, Nd, Sm, and Gd in Figures 1−6 will be employed for the identification of new nitrides and dinitrogen complexes.

Discussion

The discussion is divided into two main portions: metal nitrides and metal dinitrogen complexes. The first portion details the identification of the four types of lanthanide nitrides observed, with a brief description of the analysis of each metal analogue. The second portion, which deals with molecular nitrogen complexed to a metal center, includes an explanation of each identified complex. Nitrogen gas samples composed of equimolar concentrations of $^{14}N_2$ and $^{15}N_2$ are termed "mixed" samples; statistical mixtures of $^{14}N_2 + {}^{14}N^{15}N + {}^{15}N_2$ are termed "scrambled" and are obtained by flowing the mixed samples through a microwave discharge, providing scrambled samples on nitrogen recombination.

Nitrides. The three true nitrides observed are of the types LnN, LnN_2, and $(LnN)_2$, also known as $Ln(\mu\text{-}N)_2Ln$. The presence of the N_3 radical in the spectra[23,24] attests that laser-ablated metal atoms carry sufficient excess energy to dissociate N_2, providing the N atoms required for formation of these products.[9,10] Contrary to transition metal experiments, N_3^- absorbs more strongly at 2003.1 cm^{-1} than does the N_3 radical at 1657.7 cm^{-1}.[9−12] It can be clearly seen that for LnN and $(LnN)_2$ species postannealing band locations in argon with added N_2 very nearly coincide with band positions found in nitrogen films, under which condition all molecules are presumed to be coordinatively saturated. This observation lends support to the conclusion that dinitrogen complexation is an adequate explanation for the shifting of these product peaks after annealing of argon matrices.[9,10]

LnN. The mononitride was obtained in nitrogen films for all six lanthanides studied and in argon for all except Eu (Table 7). The primary diagnostics for the mononitrides are the nitrogen $^{14}N/^{15}N$ isotopic frequency ratios, which are just smaller than ratios approximated by the harmonic oscillator, and the doublet of peaks for both the mechanically mixed and scrambled nitrogen isotopic samples (Figure 2), which denotes the participation of exactly one N atom. As can be seen from Table 7, only NdN, SmN, and GdN were obtained in sufficient quantities in argon matrix experiments to observe intermediate and saturated complexes in samples containing 2% N_2. Note that the LnN fundamentals fall near the corresponding monoxide values.[25−27]

In addition to the diagnostics for the mononitride in N_2-containing experiments, further evidence for the mononitride identifications is found in experiments containing NO reacted with the same lanthanide metals.[25] As shown in Table 7, the mononitrides of all of the studied lanthanides except Eu have been confirmed by isolation in argon after reaction with NO. This is an important point because the NO experiments were typically performed with 0.2% NO mixtures in argon. Therefore, it is highly unlikely that the absorptions observed in these NO experiments are due to complexed molecules.

It is noted upon examination of Table 7 that the experimental isotopic ratios derived from argon matrix experiments are invariably smaller than the harmonic oscillator ratios, whereas the experimental nitrogen film ratios are often larger than the argon matrix values. The decrease in value of the isotopic ratio from the harmonic oscillator to the argon matrix is accounted for by anharmonicity in the molecular vibration that is unaccounted for by the harmonic model. The increase from argon matrices to nitrogen films is due to a damping of the metal motion by N_2 ligation, effectively increasing the mass of the metal, thereby increasing the nitrogen participation in the vibration and the nitrogen isotopic ratio.

TABLE 1: Product Absorptions (cm^{-1}) Observed for Laser-Ablated Ce Atoms in Solid Matrices at 10 K

$^{14}N_2$	$^{15}N_2$	$^{14}N_2 + {}^{15}N_2$	$^{14}N_2 + {}^{14}N^{15}N + {}^{15}N_2$	$R(^{14}N/^{15}N)^b$	anneal[c]	identity
			Argon[a]			
2327.0	2249.0	2326.8, 2249.0		1.0347	+++	N_2
2316.8	2239.9	2316.5, 2239.9	2316.9, 2278.6, 2239.9	1.0343	a+++	$(NN)_x(CeN)_2$
2262.5	2188.8			1.0337	b++	$(NN)_xCeO$
2175	2102	2174	2174.6, 2138.6, ...	1.0347	a+++	$(NN)_xCeO_2$
2115.1	2045.5	2112, 2045	2109, 2077, 2040	1.0340	b++	$Ce(NN)_x$
2090.4	2021.9			1.0339	b++	$Ce(NN)_x$
2055.5	1988.1			1.0339	b+−	$Ce(NN)_x$
2018.7	1952.5			1.0339	b+−	$Ce(NN)_x$
1987.0	1922.3			1.0337	b+−	$Ce(NN)_x$
1865.2	1803.7	1865, 1838, 1804	1864, 1847, 1833, 1816, 1804	1.0341	b++(−)	?
1800.7	1741.1	1800.9, 1751.1, 1741.1,		1.0342	a++0	?
1770.2	1711.7	(1796.6), 1770.4, 1729.4, 1711.7	1770.4, 1752.2, 1741.3, 1729.1, 1722.9, 1711.7	1.0342	a+00	$Ce(NN)_2$
1765.5	1707.2	(1796.5), 1764.9, 1721.8, 1706.6	1765.5, 1746.5, 1736.6, 1722.8, 1717.9, 1707.2	1.0341	b++	$(NN)_xCe(NN)_2$
1608.7	1561.9	1608.7, 1578.5, 1561.9	1608.6, 1595.0, 1585.1, 1578.3, 1572.5, 1562.1	1.0300	a++−	$Ce^+(N_2)_2^-$
1569.1	1517.3	1569.1, 1517.3	1569.1, 1542.6, 1517.3	1.0341	a++0	Ce(NN)
843.3	817.7	843.4, 817.9	843.4, 817.6	1.0313	a+− −	CeN
808.6	808.5				a0− −	CeO
790.9	768.9	791.0, 768.7	791.1, 781.6, 768.8	1.0286	a0- -	CeN_2
757.2	757.2				a++0	$(NN)_xCeO$
736.9	736.9				a− − −	CeO_2
714.8	714.1				b++	$(NN)_xCeO_2$
667.6	647.4	667.4, 647.3	667.7, 657.9, 647.5	1.0312	a+− −	$(CeN)_2$ (B_{3u})
664.4	644.4	664.5, 644.4	664.7, 654.9, 644.7	1.0310	a− − −	$(NN)_x(CeN)_2$ (B_{3u})
662.0	642.3	661.9, 642.2	661.9, 652.2, 642.3	1.0307	a− − −	$(NN)_x(CeN)_2$ (B_{3u})
637.7	618.2	636.8, 617.9	638.9, 629.5, 619.3	1.0315	b++	$(NN)_x(CeN)_2$ (B_{3u})
542.8	526.7	542.6, 526.7	542.8, 533.0, 526.4	1.0306	a− − −	$(CeN)_2$ (B_{2u})
538.8	523.3	538.3, 523.2	538.9, 530.1, 523.3	1.0296	a− − −	$(NN)_x(CeN)_2$ (B_{2u})
534.7	519.5	534.4, 519.5	534.3, 526.1, 519.5	1.0293	b+−	$(NN)_x(CeN)_2$ (B_{2u})
526.0	510.1	526.1, 510.9	526.0, 517.1, 510.1	1.0312	b++	$(NN)_x(CeN)_2$ (B_{2u})
			Dinitrogen[a]			
3540	3423			1.034	b++	$(NN)_xCe(NN)_2$
2327.7	2249.8	2327.9, 2249.9	2327.7, 2289.0, 2250.1	1.0346	a−00	N_2
2175.8					a0− −	?
2130	2060	2128, 2064	2098	1.0340	a− −0	$Ce(NN)_x$
2003.3	1937.5				a− − −	N_3^-
1828.9	1768.6	1827.0, 1767.2	1826.3, 1797.8, 1767.5	1.0341	a− − −(+)	?
1760.5	1702.3	1760.0, 1715.6, 1702.1	1759.8, 1740.5, 1731.2, 1715.4, 1712.8, 1701.7	1.0342	a+++	$(NN)_xCe(NN)_2$
1657.6	1603.3				a− − −	N_3
1563.0	1511.4	1562, 1535, 1510	1562, 1548, 1536, 1523, 1513, 1510	1.0341	a++0(−)	$(NN)_xCe^+(N_2)_2^-$
1411.6	1385.5	1411.6, 1385.5	1411.6, 1385.5	1.0188	a+++(−)	$(NN)_xCeNO$
1402.8	1377.3	1402.8, 1377.3	1402.8, 1377.3	1.0185	a+++(−)	$(NN)_xCeNO$
851.7	826.3	851.5, 825.9	851.5, 825.9	1.0307	a− − −(+)	?
789.4	765.1			1.0318	a++0	$(NN)_xCeN$
772.1	748.4	771.8, 748.4	771.8, 748.4	1.0317	a++0	$(NN)_xCeN$
756.4	735.1	756.2, 747.3, 735.2	756.2, 747.3, 735.2	1.0290	a+++	$(NN)_xCeN_2$
729.9	726.1	729.9, 726.1	729.9, 726.1	1.0052	a++−	$(NN)_xNCeO$
728.7	724.9	728.7, 724.9	728.7, 724.9	1.0052	a++−	$(NN)_xNCeO$
719.1	719.1	719.1	719.1		a++−	$(NN)_x(CeO_2)$
714.6	714.6				a+− −	$(NN)_x(CeO_2)$
639.6	620.2	639.6, 628.5, 620.2	639.6, 628.5, 620.2	1.0313	a+− −	$(NN)_x(CeN)_2$ (B_{3u})
526.2	509.8	526.2, 516.8, 509.8	526.2, 516.8, 509.8	1.0322	a+− −	$(NN)_x(CeN)_2$ (B_{2u})

[a] Matrix host. [b] Ratio ($^{14}N/^{15}N$) isotopic frequencies. [c] Annealing behavior: "a" denotes presence on deposition; +, −, or 0 indicates the direction of growth in three successive annealings; "b" denotes appearance on the first annealing; +, −, or 0 indicates changes on second and third annealings; (+) or (−) indicates changes on photolysis.

CeN. In $^{14}N_2$ films a strong sharp peak at 772.1 cm^{-1} that increases with annealing but is not significantly affected by photolysis is assigned to the stretching vibration of CeN contained in an N_2 cage. Its ^{15}N counterpart is found at 748.4 cm^{-1} and exhibits parallel photolytic and annealing behavior. Both of these peaks are found, without additional counterparts, in the mixed and scrambled nitrogen films. This verifies that only one N atom is involved in the observed motion, and the agreement between the experimental nitrogen isotopic ratio and the approximated harmonic oscillator nitrogen isotopic ratio confirms the assignment to CeN.

The frequency of $Ce^{14}N$ ($Ce^{15}N$) can be observed in solid argon at 843.3 (817.7) cm^{-1}. The peak pattern for mixed and scrambled isotopic nitrogen samples in argon is the same as in nitrogen. In argon CeN absorptions decrease with successive annealing and are not significantly affected by photolysis. The gas-phase value of $Ce^{14}N$ is expected to occur at 850 ± 10 cm^{-1}.

PrN. The sharp nitrogen film peak at 788.0 (763.6) cm^{-1} is assigned to $Pr^{14}N$ ($Pr^{15}N$) (Figure 2). In argon matrices, the analogous peak is found at 857.9 (831.6) cm^{-1}. As with CeN, the concentration of PrN in the matrix increases concurrently with the annealing of nitrogen films. This is expected because

TABLE 2: Product Absorptions (cm^{-1}) Observed for Laser-Ablated Pr Atoms in Solid Matrices at 10 K

$^{14}N_2$	$^{15}N_2$	$^{14}N_2 + {}^{15}N_2$	$^{14}N_2 + {}^{14}N^{15}N + {}^{15}N_2$	$R(^{14}N/^{15}N)^b$	anneal[c]	identity
			Argon[a]			
2314.4	2237.4	2314.0, 2236.7	2314.2, 2275.9, 2237.1	1.0344	b++	$(NN)_x(PrN)_2$
2164.8	2092.7			1.0345	b++	$(NN)_xPrO_2$
2115.2	2045.4	2111.7, 2101.9, 2041.4		1.0341	b++	$Pr(NN)_x$
2107.3	2037.7	2107.0, 2095.7, 2037.8		1.0342	b++	$Pr(NN)_x$
2029.9	1963.0			1.0341	b− −	$Pr(NN)_x$
1989.7	1923.4			1.0345	b− −	$Pr(NN)_x$
1803.4	1743.4	1803.4, 1798.3, 1753.1, 1743.3		1.0344	a+0−	$(NN)Pr(N_2)$
1768.0	1709.5	1768.0, 1726.0, 1709.5	1767.7, 1750.1, 1739.0, ..., 1720.9, 1709.5	1.0342	a++0	$Pr(NN)_2$
1767.1	1708.6	(1803.7), 1766.8, 1724.9, 1708.4	1766.9, 1748.0, 1737.8, 1724.9, 1719.1, 1708.4	1.0342	b++	$(NN)_xPr(NN)_2$
1582.8	1535.8	1583.6, 1554.6, 1536.4	..., 1569.1, 1560.5, 1554.4, 1547.3, 1536.3	1.0306	a− − −	$Pr^+(N_2)_2^-$
857.9	831.6	857.9, 831.6	857.9, 831.6	1.0316	a00−	PrN
843.0		842.9	843.0		a+0−	$(NN)_xPrN$
816.9	816.9	816.9	816.9		a− − −	PrO
772.7	772.6	772.6	772.6		a+− −	$(NN)_xPrO$
730.1	730.1	730.1	730.1		a+0−	PrO_2
711.7	711.7				b++	$(NN)_xPrO_2$
670.1, 621.0	654.5, 614.5	(669.7, 620.9), (654.1, 614.9)	(669.7, 620.9), (661.9, 617.6), (654.1, 614.9)	1.0238, 1.0106	a0− −	$(PrN)_2$ (B_{3u}, $B_{3g} + B_{1u}$)
666.8, 639.8	648.5, 621.8	(666.7, 639.7), (648.4, 621.9)	(666.1, 639.7), (630.8), (648.4, 622.0)	1.0282, 1.0289	b++	$(PrN)_2$ (B_{3u}, $B_{3g} + B_{1u}$)
639.8	621.8	639.7, 621.9	639.7, 630.8, 622.0	1.0289	b++	$(PrN)_2$ (B_{3u})
570.6	554.1	broad 567.9	broad 565.3	1.0298	a0− −	$Pr_y(NN)_x$
544.9	528.4	544.8, 528.3	544.9, 535.4, ...	1.0312	a− − −	$(PrN)_2$ (B_{2u})
540.2	523.8	540.2, 523.9	540.2, 531.2, 523.9	1.0313	a+− −	$(NN)_x(PrN)_2$ (B_{2u})
537.6	521.3	537.6, 521.3	537.5, 528.5, 521.4	1.0313	a++-	$(NN)_x(PrN)_2$ (B_{2u})
531.0	514.9	531.3, 515.2	531.1, 521.3, 515.3	1.0313	b++	$(NN)_x(PrN)_2$ (B_{2u})
529.4	513.4	529.3, 513.3	529.2, 520.3, 513.2	1.0312	b++	$(NN)_x(PrN)_2$ (B_{2u})
475.7	461.2	475.6, 460.6	475.2, 460.5	1.0314	a− − −	Pr_2N
			Dinitrogen[a]			
3541	3421			1.035		$(NN)_xPr(NN)_2$
2318.1	2240.5	2318.8, 2240.4	2318.9, 2280.4, 2240.2	1.0346	a000	$(NN)_x(PrN)_2$
2135.8	2065.2	2136.2, 2065.7	2098.2	1.0342	a− − −	$Pr(NN)_x$
1760.0	1701.7	(1792.3), 1760.2, 1716.6, 1701.7	1760.0, 1741.7, 1731.6, 1716.9, 1712.3, 1701.7	1.0343	a− − −	$(NN)_xPr(NN)_2$
1561.0	1508.9	1560, ..., 1509		1.0345	a0− −(−)	$(NN)_xPr^+(N_2)_2^-$
1538.6	1488.1	1539, 1523, 1488		1.0339	a++−(−)	$(NN)_xPr^+(N_2)_2^-$
880.5	859.6	880.4, 859.6	880.4, 859.7	1.0243	b++	$(NN)_xNPrO$
877.5	856.8	877.2, 856.8	877.7, 856.9	1.0242	b++	$(NN)_xNPrO$
809.6	786.8	809.4, 800.0, 787.1	809.6, 800.0, 786.8	1.0290	a++−	$(NN)_xPrN_2$
806.8	782.0	806.8, 782.0	806.8, 782.1	1.0317	a+− − (+)	$(NN)_xPrN$
788.0	763.6	788.0, 763.6	788.0, 763.6	1.0320	a++−	$(NN)_xPrN$
729.0	722.3	729.0, 722.3		1.0093	b++	$(NN)_xNPrO$
727.7	720.3	727.7, 720.3		1.0103	b++	$(NN)_xNPrO$
722.4	722.4	722.4	722.4		b++	$(NN)_xPrO_2$
531.1	514.9	531.1, 522.1, 514.9	531.1, 522.1, 514.9	1.0315	a0− −	$(NN)_x(PrN)_2$ (B_{2u})

[a] Matrix host. [b] Ratio ($^{14}N/^{15}N$) isotopic frequencies. [c] Annealing behavior: "a" denotes presence on deposition; +, −, or 0 indicates the direction of growth in three successive annealings; "b" denotes appearance on the first annealing; +, −, or 0 indicates changes on second and third annealings; (+) or (−) indicates changes on photolysis.

of the presence of N atoms in the film, which can react when diffusion is allowed. In nitrogen, PrN increases incrementally with annealing cycles, but in argon it decreases gradually. The predicted gas-phase value of $Pr^{14}N$ is 865 ± 10 cm^{-1}.

NdN. $Nd^{14}N$ ($Nd^{15}N$) is found in nitrogen films at 782.5 (758.2) cm^{-1}. The absorption increases with annealing but is unchanged with photolysis. In argon films NdN absorbs at 853.3 (827.2) cm^{-1} and decreases with annealing while remaining unchanged by photolysis. After 42 K annealing of argon matrices, $(NN)_x$NdN absorbs at 780.3 (756.3) cm^{-1}, very near the nitrogen film value, while the original peaks upon deposition have decreased considerably. The red shift of the absorption is due to N_2 complexation of the mononitride and will be delineated more fully in the GdN case, for which the data are most clear. $Nd^{14}N$ is predicted to occur in the gas phase at 860 ± 10 cm^{-1}.

SmN. In nitrogen films, a strong absorption at 768.6 (745.2) cm^{-1} that increases with annealing is assigned to $Sm^{14}N$ ($Sm^{15}N$). The clear nitrogen isotopic doublet for mixed and scrambled nitrogen samples and the close agreement of the experimental isotopic ratio with the calculated harmonic oscillator ratio positively identify this species. In argon, very weak bands seen at 822.6 (797.3) cm^{-1} before annealing and 769.3 (745.6) cm^{-1} after are assigned to SmN and $(NN)_x$SmN, respectively. This allows a gas-phase prediction for $Sm^{14}N$ of 830 ± 10 cm^{-1}.

EuN. Although no appreciable quantity of europium nitrides was formed in reactions of laser-ablated atomic Eu with N_2, a weak absorption found in nitrogen films at 776.5 (752.4) cm^{-1} is attributed to $Eu^{14}N$ ($Eu^{15}N$). Although these absorptions were observed in neither mixed nor scrambled films, in the pure isotopic $^{14}N_2$ and $^{15}N_2$ samples, they demonstrate

TABLE 3: Product Absorptions (cm^{-1}) Observed for Laser-Ablated Nd Atoms in Solid Matrices at 10 K

$^{14}N_2$	$^{15}N_2$	$^{14}N_2 + {}^{15}N_2$	$^{14}N_2 + {}^{14}N^{15}N + {}^{15}N_2$	$R(^{14}N/^{15}N)^b$	anneal[c]	identity
			Argon[a]			
2318.9	2241.5	2318.9, 2241.4	2319.4, 2280.7, 2241.8	1.0345	b++	$(NN)_x(NdN)_2$
2162.4	2091.0	2162.5, 2091.0		1.0341	b++	$(NN)_xNdO_2$
2112.7	2042.8			1.0342	b++	$Nd(NN)_x$
2104.2	2034.7	2105.4, 2038.5	2107, 2072, 2040	1.0342	b++	$Nd(NN)_x$
1813.4	1753.1			1.0344	a++−	?
1805.2	1745.2	1805.2, 1798.4, ..., 1745.0		1.0344	a− − −	$(NN)Nd(N_2)$
1761.0	1702.6	(1801.9), 1760.6, 1719.3, 1702.3	1760.5, 1742.2, 1731.9, 1720.0, 1713.2, 1702.5	1.0343	b++	$(NN)_xNd(NN)_2$
1759.2	1701.2	(1800.5), 1759.2, 1719.7, 1701.2	1760.5, 1741.9, 1730.4, 1720.0, 1712.9, 1701.2	1.0341	a+− −	$Nd(NN)_2$
1566.0	1516.6	1566.1, 1536.1, 1516.7	1565.9, 1552.1, 1541.4, 1535.8, 1527.6, 1516.4	1.0326	a− − − (−)	$Nd^+(N_2)_2^-$
1234.7	1207.5	1234.7, 1207.4		1.0225	a0− −	Nd(NO)
853.3	827.2	853.4, 827.2	853.3, 827.1	1.0316	a− − −	NdN
837.9		838.0	837.9		a00−	$(NN)_xNdN$
814.0	814.0				a− − −	NdO
780.8	756.7	780.3, 756.3		1.0318	b++	$(NN)_xNdN$
771.6	771.6	771.5	771.5		a− − −	$(NN)_xNdO$
716.0	716.0				a− − −	NdO_2
695.5	695.5				b++	$(NN)_xNdO_2$
679.2	659.1	679.1, 659.1	679.5, 669.6, 659.5	1.0305	a− − −	$(NdN)_2$ (B_{3u})
677.6	657.4	677.2, 657.0	677.5, 667.4, 657.5	1.0307	a− − −	$(NN)_x(NdN)_2$ (B_{3u})
673.6	654.6	674.2, 655.6	673.8, 664.4, 654.8	1.0290	b++	$(NN)_x(NdN)_2$ (B_{3u})
657.5	637.9			1.0307	b++	$(NN)_x(NdN)_2$ (B_{3u})
546.7	530.1	546.8, 530.2	547.0, 538.2, 530.3	1.0313	a− − −	$(NdN)_2$ (B_{2u})
542.4	526.0	542.3, 526.0	542.3, 533.2, 526.0	1.0312	a− − −	$(NN)_x(NdN)_2$ (B_{2u})
539.4	523.0	539.3, 522.9	539.3, 531.5, 523.0	1.0314	a+− −	$(NN)_x(NdN)_2$ (B_{2u})
535.5	519.3	535.5, 519.2	535.2, 527.1, 519.3	1.0312	a++−	$(NN)_x(NdN)_2$ (B_{2u})
529.7	513.6	529.5, 513.3	529.5, ..., 513.4	1.0313	b++	$(NN)_x(NdN)_2$ (B_{2u})
477.4	463.6	476.6 463.6	477.1, 463.8	1.0298	a− − −	Nd_2N
			Dinitrogen[a]			
3540	3422			1.034	a− − −	$(NN)_xNd(NN)_2$
2317.5	2240.1	2317.5, 2240.1	2317.5, 2278.9, 2240.2	1.0346	a− − −	$(NN)_x(NdN)_2$
2125.3	2055.6	2122.7, 2060.7	2092.5	1.0339	a− − −	$Nd(NN)_x$
1756.3	1697.9	(1793.3), 1755.4, 1711.5, 1697.4	1755.9, 1736.1, 1726.5, 1711.2, 1708.6, 1695.9	1.0344	a0+−	$(NN)_xNd(NN)_2$
1566.3	1514.9	1566.3, 1541.5, 1515.3		1.0339	a+0−(−)	$(NN)_xNd^+(N_2)_2$-
1545.3	1495.0	1546.8, 1527.8, 1495.7		1.0336	a++−(−)	$(NN)_xNd^+(N_2)_2^-$
1252.9	1226.6			1.0214	a− − −	$(NN)_xNdNO$
1177.2	1149.7			1.0239	a− − −	$(NN)_xNdNO$
782.0	758.1	782.0, 758.1	782.0, 758.1	1.0315	a++0	$(NN)_xNdN$
778.4	756.7	778.2, 768.3, 756.5	778.2, 768.3, 756.5	1.0287	a++0	$(NN)_xNdN_2$
706.6	706.6				a+++	$(NN)_xNdO_2$
694.0	694.0				a+− −	$(NN)_xNdO_2$
657.6	638.0	657.6, 648.6, 638.0	657.9, 648.6, 638.4	1.0307	a− − −	$(NN)_x(NdN)_2$ (B_{3u})
530.3	514.0	530.3, 521.4, 514.0	530.6, 521.7, 514.3	1.0317	a− − −	$(NN)_x(NdN)_2$ (B_{2u})

[a] Matrix host. [b] Ratio ($^{14}N/^{15}N$) isotopic frequencies. [c] Annealing behavior: "a" denotes presence on deposition; +, −, or 0 indicates the direction of growth in three successive annealings; "b" denotes appearance on the first annealing; +, −, or 0 indicates changes on second and third annealings; (+) or (−) indicates changes on photolysis.

characteristic growth on annealing and exhibit a nitrogen isotopic ratio in good agreement with the harmonic oscillator approximation. EuN is not observed in argon matrices, but its value in argon can be approximated from the nitrogen film frequency. The gas-phase value is predicted to be 830 ± 10 cm^{-1}.

GdN. GdN is readily observed both in argon and in nitrogen matrices. In nitrogen films a prominent sharp peak at 752.7 (729.3) cm^{-1} is assigned to $Gd^{14}N$ ($Gd^{15}N$). Intermediate components are absent in both the mixed and scrambled nitrogen isotopic samples, and there is characteristic growth upon annealing of the films. The experimental isotopic ratio of 1.0319 is clearly in agreement with the approximated harmonic oscillator ratio of 1.0320. In argon films, a weak peak at 797.0 (772.5) cm^{-1} is assigned to isolated GdN, while several peaks red-shifted from the initial absorption are assigned to $(NN)_xGdN$, with various values of x ranging to complete ligation of GdN as seen in the nitrogen films (Figure 3). As shown in Figure 3, the initial peaks decrease with annealing until at 45 K they are completely absent and the only remaining peak is a strong absorption at 752.7 (729.4) cm^{-1}, identical to the value of the nitrogen film peak displayed above it. This demonstrates visually the stepwise complexation of the mononitride molecule by N_2 ligands. $Gd^{14}N$ is predicted to absorb in the gas phase at 810 ± 10 cm^{-1}.

LnN_2. The LnN_2 molecule was observed in nitrogen films for Ce, Pr, Nd, and Sm but could be identified in argon only for Ce. Key identifiers for these molecules were the $^{14}N/^{15}N$ ratios, which were in all cases in excellent agreement with the harmonic antisymmetric stretching values for linear N−Ln−N (1.0289−1.0293 for Ce−Sm), and the isotopic triplets of peaks invariably observed with isotopically scrambled N_2 samples (Figure 2), which is a clear indicator that exactly two N atoms are involved in the vibrational modes. The nitrogen isotopic

TABLE 4: Product Absorptions (cm^{-1}) Observed for Laser-Ablated Sm Atoms in Solid Matrices at 10 K

$^{14}N_2$	$^{15}N_2$	$^{14}N_2 + {}^{15}N_2$	$^{14}N_2 + {}^{14}N{}^{15}N + {}^{15}N_2$	$R(^{14}N/^{15}N)^b$	anneal[c]	identity
			Argon[a]			
2306.3	2230.4	2309.3, 2233.2	2308.2, 2270.3, 2232.9	1.0340	a+++	$(NN)_x(SmN)_2$
2101.9	2033.3	2099.0, 2032.0		1.0337	a+++	$Sm(NN)_x$
1812.9	1753.6	1812.7 1789.4, 1753.6		1.0338	a+++	
1785.8	1728.5			1.0332	a+++	
1749.1	1691.2	(1784.0), 1751.5, 1706.4, 1693.3		1.0342	b++	$(NN)_xSm(NN)_2$
1744.9	1687.0	1745.0, 1687.2	1745.0, 1716.2, 1687.0	1.0343	a++0	$Sm(N_2)$
1742.6	1685.1	(1781.0), 1742.7, 1703.0, 1685.1	1742.7 1725.2, 1714.1, 1703.1, 1696.4, 1685.1	1.0341	a− − −	$Sm(NN)_2$
822.6	797.3	822.5, 797.2	822.6, 797.7	1.0317	a0− −	SmN
818.4	818.4	818.4	818.5		a+0−	SmO
769.3	745.6	768.6, 745.1		1.0318	b++	$(NN)_xSmN$
686.7	665.8	686.7, 665.9	686.7, 676.5, 665.7	1.0314	a0− −	$(SmN)_2$ (B_{3u})
685.0	664.0	684.9, 664.2	685.0, 674.8, ...	1.0316	a− − −	$(NN)_x(SmN)_2$ (B_{3u})
683.2	662.4	683.2, 662.2	683.2, 673.0, 662.0	1.0314	a− − −	$(NN)_x(SmN)_2$ (B_{3u})
681.1	660.5	681.0, 660.3	683.2 671.3, 662.4	1.0312	b+−	$(NN)_x(SmN)_2$ (B_{3u})
679.1	658.4	679.2, 658.3		1.0314	b++	$(NN)_x(SmN)_2$ (B_{3u})
663.8	643.3	663.2, 643.1		1.0319	b0+	$(NN)_x(SmN)_2$ (B_{3u})
553.9	537.0	554.1, 537.7		1.0315	a− − −	$(SmN)_2$ (B_{2u})
550.9	534.0	550.9, 534.0	550.7, 541.2, 533.8	1.0316	a0− −	$(NN)_x(SmN)_2$ (B_{2u})
548.3	531.1	548.2, 531.0		1.0324	a+− −	$(NN)_x(SmN)_2$ (B_{2u})
545.5	528.6			1.0320	a++−	$(NN)_x(SmN)_2$ (B_{2u})
539.7	522.1	537.8, 520.9		1.0337	b++	$(NN)_x(SmN)_2$ (B_{2u})
			Dinitrogen[a]			
3522.2	3406.3			1.0340	a+00(+)	$(NN)_xSm(NN)_2$
3479.4	3365.5	3478.5, 3365.1		1.0338	a−00	$(NN)_xSm(N_2)$
2311.8	2234.5	2311.4, 2234.4	2311.8, 2273.4, 2235.5	1.0346	a++0	$(NN)_x(SmN)_2$
2122	2056		2084	1.0321	a− − −	$Sm(NN)_x$
2090	2022	2087, 2022		1.0336	a− − −	$Sm(NN)_x$
1937	1875	1933, 1873	1935, 1905, 1874	1.0331	a0+−	?
1750.3	1692.9	1749.8, 1693.2	1749.8, 1722.0, 1693.3	1.0339	a− − −	$(NN)_xSm(N_2)$
1747.4	1689.5	(1779.1), 1747.4, 1704.2, 1689.5	1747.4, 1728.7, 1718.6, 1704.1, 1699.6, 1689.5	1.0343	a+− −(+)	$(NN)_xSm(NN)_2$
1576.8	1525.0	1577, 1525	1577, 1551, 1525	1.0340	a++−	Sm(NN)
1361.5	1316.0			1.0346	b++	$Sm_y(NN)_x$
768.6	745.2	768.5, 745.2	768.6, 745.2	1.0314	a++0	$(NN)_xSmN$
738.1	717.3	738.0, 728.2, 717.4	737.9, 728.2, 717.3	1.0290	a+++	$(NN)_xSmN_2$
706.2	683.3			1.0335	a++−	?
666.5	646.0	666.4, 656.4, 646.1	666.3, 656.2, 645.6	1.0317	a++−	$(NN)_x(SmN)_2$ (B_{3u})
621.2	621.2				a++−	$(NN)_xSmO_2$
533.9	516.7			1.0333	a− − −	$(NN)_x(SmN)_2$ (B_{2u})
526.7	511.2			1.0303	b++	$(NN)_x(SmN)_2$ (B_{2u})

[a] Matrix host. [b] Ratio ($^{14}N/^{15}N$) isotopic frequencies. [c] Annealing behavior: "a" denotes presence on deposition; +, −, or 0 indicates the direction of growth in three successive annealings; "b" denotes appearance on the first annealing; +, −, or 0 indicates changes on second and third annealings; (+) or (−) indicates changes on photolysis.

ratios of the experimentally observed peaks indicate that the dinitrides, LnN_2, are linear, or very nearly linear, molecules.

CeN_2. CeN_2 in nitrogen exhibits an isotopic triplet at 756.2, 747.3, 735.2 cm^{-1} in both the mixed and scrambled nitrogen samples and increases with annealing but changes little with photolysis. A weak absorption at 790.9 (768.9) cm^{-1} in the argon matrix experiments is assigned to $Ce^{14}N_2$ ($Ce^{15}N_2$) and does not increase with annealing but does increase with photolysis (Figure 4). Two isotopic peaks are present in the mixed-nitrogen samples with argon, and a central component appears at 781.6 cm^{-1} with scrambled nitrogen samples in argon. Note that in mixed-nitrogen films three isotopic nitrogen peaks are present for the CeN_2 molecule, but in argon matrices with mixed-nitrogen samples, only two nitrogen isotopic peaks are present.

The experimental nitrogen isotopic ratio of 1.0286 in argon is slightly smaller than the harmonic antisymmetric stretching ratio of 1.0289 for a linear N−Ce−N molecule. This provides evidence that the molecule likely has linear geometry. As with the mononitrides, the experimental ratio of the dinitride in solid nitrogen, 1.0290, is larger than that in solid argon. This is due to the effective decrease in metal motion due to N_2 ligation of the metal center.

Cerium results shown in Figure 4 clearly demonstrate the mixed isotopic doublet for CeN_2 in argon, but like PrN_2 (Figure 2), CeN_2 exhibits a mixed isotopic triplet in N_2. The reaction mechanism therefore includes a single N_2 molecule upon formation of LnN_2 in argon but incorporates atoms from two separate N_2 molecules when synthesis occurs in a nitrogen film. Two mechanisms are proposed that explain these observations; the first dominates in argon matrices, reactions 1 and 2, and the second in nitrogen matrices, reactions 3 and 4. These pathways are demonstrated using the results of cerium nitride DFT calculations to obtain relative energies of the reactants and products involved.[28]

$$Ce + N_2 \rightarrow Ce(N_2) \qquad \Delta E = -1.791 \text{ eV} \qquad (1)$$

$$Ce(N_2) + h\nu \rightarrow CeN_2 \qquad \Delta E = -0.031 \text{ eV} \qquad (2)$$

$$Ce + N_2 \rightarrow CeN + N \qquad \Delta E = +3.303 \text{ eV} \qquad (3)$$

$$CeN + N \rightarrow CeN_2 \qquad \Delta E = -5.125 \text{ eV} \qquad (4)$$

Step 2 in the first mechanism is facilitated by UV light, as can

TABLE 5: Product Absorptions (cm^{-1}) Observed for Laser-Ablated Eu Atoms in Solid Matrices at 10 K

$^{14}N_2$	$^{15}N_2$	$^{14}N_2 + {}^{15}N_2$	$^{14}N_2 + {}^{14}N^{15}N + {}^{15}N_2$	$R(^{14}N/^{15}N)^b$	anneal[c]	identity
			Argon[a]			
2303.3	2226.5	2300.4, 2224.0	2300.1, 2262.9, 2227.4	1.0345	b++	$Eu(NN)_x$
1812.4	1752.9			1.0339	a− − −	$Eu_x(NN)_y$
1787.5	1725.1	1784.1, 1725.0	1740	1.0362	b++	$Eu(N_2)$
667.9	667.8	667.8	667.8		a− − −	EuO
			Dinitrogen[a]			
3511.2	3395.6			1.0340	a− − −	$(NN)_xEu(NN)_2$
3465.2	3351.0	3464.5, 3352.6	3465.6, 3409.4, 3352.8	1.0341	a+0−	$(NN)_xEu(N_2)$
2307.2	2230.3	2307.3, 2230.4	2307.7, 2269.1, 2230.5	1.0345	a00−	$(NN)_xEuN$
2119	2050	2080	2082	1.0337	a− − −	$Eu(NN)_x$
2082	2015	2082, 2014	2082.0	1.0333	a− − −	$Eu(NN)_x$
1743.5	1686.1	1743, 1686	1743, 1715, 1686	1.0340	a00−	$(NN)_xEu(N_2)$
1742.2	1684.6	(1773.2), 1742.2, 1699.3, 1684.8	1742.2, 1723.7, 1713.7, 1699.6, 1694.7, 1685.4	1.0342	a− − −	$(NN)_xEu(NN)_2$
1490	1440	1490, 1462, 1441	1464	1.0346	a00−	$Eu_y(NN)_x$
1350	1306	1349, 1323, 1305		1.0337	a000	$Eu_y(NN)_x$
776.5	752.4			1.0320	a++−	$(NN)_xEuN$
735.2	711.5	735.5, 711.8	735.1, 711.8	1.0333	a0− −	?
684.9	664.4	684.9, 664.1	684.6 664.0	1.0309	a++0	?
630.3	630.3	630.3	630.3		a+0−	$(NN)_xEuO$
451.3	437.3	451.1, 438.0	451.0, 437.5	1.0320	a+− −	$(NN)_xEu_2N$

[a] Matrix host. [b] Ratio ($^{14}N/^{15}N$) isotopic frequencies. [c] Annealing behavior: "a" denotes presence on deposition; +, −, or 0 indicates the direction of growth in three successive annealings; "b" denotes appearance on the first annealing; +, −, or 0 indicates changes on second and third annealings; (+) or (−) indicates changes on photolysis.

be seen from the increased intensity of the CeN_2 absorptions in argon following UV photolysis (Figure 4). The second mechanism is disfavored in argon matrices because of the low level of CeN formation upon deposition (step 3) with 2−4% N_2. Because sufficient CeN is produced upon deposition in nitrogen films, step 4 becomes very important in the formation of CeN_2 in nitrogen films, where atomic N is also present. The weak intensity of CeN_2 in argon matrices testifies to the inefficiency of the first mechanism. The calculated energies show that the thermodynamic driving force of step 2 is weak. Therefore, most of the $Ce(N_2)$ formed does not progress to CeN_2 but rather remains in its initial state or forms the rhombic ring, as will be discussed in the $(LnN)_2$ section.

PrN_2. The absorption found at 809.6 (786.8) cm^{-1} in the $^{14}N_2$ ($^{15}N_2$) film is assigned to PrN_2 (Figure 2). Owing to reaction step 4, as demonstrated previously for CeN_2, this peak increases with annealing. PrN and N are known to be in the praseodymium−nitrogen films, as demonstrated previously. The isotopic nitrogen triplet in both mixed and scrambled nitrogen films (Figure 2) indicates that akin to CeN_2 the primary method of formation of PrN_2 in solid nitrogen is the second mechanism. The experimental nitrogen isotopic ratio for this absorption is 1.0290, in close agreement with the approximated harmonic value of 1.0289 for a linear N−Pr−N molecule. It is expected therefore that the NPrN molecule is linear. Finding an experimental ratio in the nitrogen films slightly in excess of the calculated harmonic value does not necessarily indicate that the molecule is bent, since ligation of the metal center by dinitrogen decreases metal motion and increases the nitrogen isotopic ratio.

NdN_2. In solid nitrogen, the matrix-split site at 778.4 (756.7) cm^{-1} is assigned to $Nd^{14}N_2$ ($Nd^{15}N_2$). Characteristic of this molecular type in solid nitrogen, the absorption increases with annealing of the film. The $^{15}N_2$ counterpart absorbs on the shoulder of the more intense $Nd^{15}N$ absorption, but its multiple site structure is still easily distinguished. The $^{14}N-Nd-^{15}N$ ν_3 vibration is observed at 768.3 cm^{-1} in both the mixed and scrambled nitrogen films. The experimental nitrogen isotopic ratio of 1.0287 is smaller than 1.0291, the harmonic oscillator ratio for linear N−Nd−N. This indicates that the molecule has linear geometry.

SmN_2. Also observed only in solid nitrogen films and matrix split like NdN_2, $Sm^{14}N_2$ ($Sm^{15}N_2$) absorbs at 738.1 (717.3) cm^{-1}. With both mixed and scrambled nitrogen isotopes a central peak is present at 728.2 cm^{-1}, showing that formation is favored by the second mechanism. The close agreement of the experimental isotopic ratio of 1.0290 with 1.0293, the harmonic oscillator ratio for a linear molecule, provides evidence for the linearity of the SmN_2 molecule that is characteristic of all four LnN_2 molecules observed.

$(LnN)_2$. This molecule type is observed for Ln = Ce, Pr, Nd, Sm, and Gd. In most cases both the B_{2u} and B_{3u} modes of these rings are identified by tracking the respective peaks through photolysis and annealing cycles, as demonstrated for neodymium samples in Figure 5. In general they exhibit nearly the same nitrogen isotopic ratios, suggesting two stretching modes of the same molecule. The harmonic oscillator isotopic nitrogen ratios approximated for the mononitride molecules, LnN, are in good agreement with the experimentally observed ratios for these peaks, which is expected for the rhombic ring molecule.[10,12] The isotopic triplets observed in the scrambled nitrogen samples confirm that exactly two N atoms participate in the observed vibrational modes.

$(CeN)_2$. Two strong, multiply split absorptions at 667.6 (647.4) and 542.8 (526.5) cm^{-1} that behave in concert through photolysis and annealing cycles are assigned to the B_{3u} and B_{2u} modes respectively of $(CeN)_2$. These bands decrease with successive annealing, while red-shifted counterparts appear and increase, demonstrating complexation of the metal centers by dinitrogen as has been shown previously for the mononitride molecules. After the final annealing, two absorptions due to the nitrogen-complexed molecule are present at 637.7 (618.2) and 526.0 (510.1) cm^{-1}, in close agreement with the nitrogen film absorptions. The nitrogen isotopic ratios agree closely with each other and with the harmonic oscillator ratio for the CeN molecule, as is expected for the rhombus. Note that in argon matrices both peaks come in pairs for mixed-nitrogen samples, while in nitrogen films, the mixed-nitrogen samples show

TABLE 6: Product Absorptions (cm^{-1}) Observed for Laser-Ablated Gd Atoms in Solid Matrices at 10 K

$^{14}N_2$	$^{15}N_2$	$^{14}N_2 + {}^{15}N_2$	$^{14}N_2 + {}^{14}N^{15}N + {}^{15}N_2$	$R(^{14}N/^{15}N)^b$	anneal[c]	identity
			Argon[a]			
2312.8	2235.6	2311.4 2238.0	2311.6, 2271.8, 2235.2	1.0345	a+++	$(NN)_x(GdN)_2$
2167.6	2096.1			1.0341	b++	?
2095.7	2026.6	2095.6, ...	2095.6, 2061.0, ...	1.0341	b++	?
2043.9	1976.5	2039.6, 1970.8	2039.4, 2005.7, 1970.8	1.0341	b++	$Gd(NN)_x$
1963.4	1898.7			1.0341	b++	?
1876.9	1814.8	1876.9, 1814.8	1876.8, 1846.0, 1814.5	1.0342	b++	$Gd(N_2)$
1741.9	1684.7	(1797.0), 1741.6, 1703.1, 1684.4	1741.7, 1724.9, 1713.3, 1703.1, 1696.2, 1684.2	1.0340	b++	$(NN)_xGd(NN)_2$
1739.6	1681.3	1739.6, 1700.0 1681.2	1739.6, ..., ..., 1699.6, 1693.0, 1681.2	1.0347	a+0−	$Gd(NN)_2$
1558.2	1506.9	1557, 1507	1554, 1533, 1508	1.0340	b++	Gd(NN)
1517.8	1467.6			1.0342	a++−	?
812.8	812.4	812.7	812.8		a− − −	GdO
797.0	772.5	797.0, 772.3	797.2, 772.9	1.0317	a− − −	GdN
785.8	761.4	785.8, 761.4	785.9, 762.0	1.0320	a+− −	$(NN)_xGdN$
768.4	745.0	768.4, 745.0	768.6, 745.0	1.0314	a+− −	$(NN)_xGdN$
761.5	738.2	761.5, 738.2	761.5, 738.5	1.0316	b+−	$(NN)_xGdN$
754.0	730.9	754.0, 730.9	754.2, 730.8	1.0316	b++	$(NN)_xGdN$
752.7	729.4	752.7, 729.4	752.9, 729.6	1.0319	b++	$(NN)_xGdN$
690.2	669.1	690.0, 668.9	689.9, 679.7, 669.1	1.0315	a− − −	$(GdN)_2$ (B_{3u})
688.3	667.2	688.0, 667.0	688.1, 677.8, 667.1	1.0316	a− − −	$(GdN)_2$ (B_{3u})
686.8	665.5	686.4, 665.4	686.5, 676.3, 665.6	1.0320	a− − −	$(GdN)_2$ (B_{3u})
681.3	660.5	681.7, 660.8	681.5, 671.6, 661.0	1.0315	b++	$(NN)_x(GdN)_2$ (B_{3u})
679.5	658.6	679.5, 658.7	679.8, 669.2, 658.6	1.0317	b++	$(NN)_x(GdN)_2$ (B_{3u})
675.7	655.0	675.4, 654.7	675.8, 665.5, 655.2	1.0316	b++	$(NN)_x(GdN)_2$ (B_{3u})
674.1	653.3	672.9, 652.3		1.0318	b++	$(NN)_x(GdN)_2$ (B_{3u})
653	633	653, 633	652, 633	1.0316	a0− −	?
589.5	571.7	589.4, 585.0, 580.7, 574.7, 572.0	589.3, 583.4, 580.9, 576.9, 572.6	1.0311	a− − − (+)	?
571.9	554.6			1.0312	a+− −	?
563.5	546.1	563.3, 546.1	563.3	1.0319	a0− −	$(GdN)_2$ (B_{2u})
560.9	543.6	560.8, 543.6	560.9	1.0318	a− − −	$(NN)_x(GdN)_2$ (B_{2u})
558.2	541.0	558.0, 540.9	558.1, 548.6, 541.1	1.0318	a0− −	$(NN)_x(GdN)_2$ (B_{2u})
554.7	537.7	554.6, 537.7	554.7, 545.3, 537.8	1.0316	a+0−	$(NN)_x(GdN)_2$ (B_{2u})
552.0	535.0	551.9, 534.8	551.1, 542.6, 535.0	1.0318	a+++	$(NN)_x(GdN)_2$ (B_{2u})
540.2	523.6	542.9, 526.2	542.8, 543.3, 526.1	1.0317	b++	$(NN)_x(GdN)_2$ (B_{2u})
538.4	521.8	538.9, 522.4	539.0, 529.7, 522.6	1.0318	b++	$(NN)_x(GdN)_2$ (B_{2u})
494.4	478.9	493.5, 478.6	494.0, 478.9	1.0324	a−0−(+)	Gd_2N
			Dinitrogen[a]			
3520	3404			1.034		$(NN)_xGd(NN)_2$
2302.9	2226.0	2303.0, 2226.2	2303.1, 2264.9, 2226.3	1.0345	a++0	$(NN)_x(GdN)_2$
2119.7	2049.6			1.0342	a+++	$(NN)_xGd(NN)_2$
2038.8	1971.6	2040.4, 1972.6	2040.0, 2006.9, 1972.6	1.0341	a− − −	$Gd(NN)_x$
1811	1751			1.0344	a000	?
1750.4	1692.3	1750.2	1750.2	1.0343	a++0	$(NN)_xGd(NN)_2$
1738.1	1680.8	1738.0, 1696.5, 1681.0	1738.2, 1721.4, 1710.1, 1695.9, 1692.5, 1681.1	1.0341	a++0(−)	$Gd(NN)_2$
1600.0	1547.2	1599, 1571, 1546		1.0341	a− − −	$Gd^+(N_2)_2^-$
1583.0	1530.7	1583, 1567, 1531		1.0342	a−0−	$Gd^+(N_2)_2^-$
1253.9	1213.1	1254.3, 1213.7	1254.3, 1233.8, 1213.5	1.0336	a000(+)	$Gd_x(N_2)$
1243.2	1202.8	1243.4, 1203.0	1243.0, 1223.4, 1202.6	1.0336	a+0−	$Gd_x(N_2)$
752.7	729.4	752.6, 729.4	752.7, 729.4	1.0319	a++0(−)	$(NN)_xGdN$
668.5	647.9	668.3, 658.4, 648.2	668.1, 658.3, 647.9	1.0318	a0+−(−)	$(NN)_x(GdN)_2$ (B_{3u})
663.8	643.4	663.7, 654.2, 643.4	663.9, 654.1, 643.4	1.0317	a0− −	$(NN)_x(GdN)_2$ (B_{3u})
545.6	529.1			1.0312	a0+0(−)	$(NN)_x(GdN)_2$ (B_{2u})
538.5	521.9	538.7, 529.3, 522.2	538.4, 529.4, 522.3	1.0318	a0− −	$(NN)_x(GdN)_2$ (B_{2u})

[a] Matrix host. [b] Ratio ($^{14}N/^{15}N$) isotopic frequencies. [c] Annealing behavior: "a" denotes presence on deposition; +, −, or 0 indicates the direction of growth in three successive annealings; "b" denotes appearance on the first annealing; +, −, or 0 indicates changes on second and third annealings; (+) or (−) indicates changes on photolysis.

isotopic triplets for both peaks. In all scrambled nitrogen samples an isotopic triplet is observed for each peak. As with the dinitrides, this behavior indicates two separate mechanisms of formation.

It can be concluded that in argon the nitrogen atoms originate from the same N_2 molecule, while in nitrogen they come from two different N_2 units. On the basis of this observation, it is proposed that when in argon, the molecule is formed via an $Ln(N_2)$ intermediate, but in nitrogen films, it is a true dimer of LnN. Since these peaks are relatively several times more intense in argon than in nitrogen, the favored method of formation of $(LnN)_2$ appears to be through the complexed intermediate rather than by dimerization of the mononitride. This is the first example of two naked lanthanide metal atoms acting in concert to complex N_2 and cleave the N−N triple bond.

Two possible mechanistic pathways are proposed, reactions 5 and 6 and reactions 7−9, both of which participate in the formation of this molecule. Results of DFT calculations for

TABLE 7: LnN and LnO Frequencies (cm^{-1}) Observed in Solid Matrices at 10 K

LnN (Ln = Ce, Pr, Nd, Sm, Eu, Gd)						
Ln	matrix[a]	$^{14}N_2$	from NO[b]	R ($^{14}N/^{15}N$)[c]	R(H.O.)[d]	LnO from NO[b]
Ce	a	843.3	843.3	1.0313	1.0317	808.4
Ce	N_2	772.1		1.0317		
Pr	a	857.9	857.9	1.0316	1.0317	816.8
Pr	N_2	788.0		1.0320		
Nd	a	853.3	853.2	1.0316	1.0317	814.3
Nd	b	780.8		1.0318		
Nd	N_2	782.0		1.0315		
Sm	a	822.6	822.7	1.0317	1.0319	808.1
Sm	b	769.3		1.0318		
Sm	N_2	768.7		1.0315		
Eu	N_2	776.5		1.0320	1.0319	668.0
Gd	a	797.0	797.1	1.0317	1.0319	812.8
Gd	b	752.7		1.0319		
Gd	N_2	752.7		1.0319		

[a] Matrix host: "a" denotes band position on deposition in an argon matrix; "b" denotes band position on conclusion of annealings in an argon matrix; N_2 denotes band position in a nitrogen matrix. [b] Frequencies observed in 0.2% NO/Ar experiments.[25] [c] Ratio ($^{14}N/^{15}N$) isotopic frequencies. [d] Ratio derived from the harmonic oscillator.

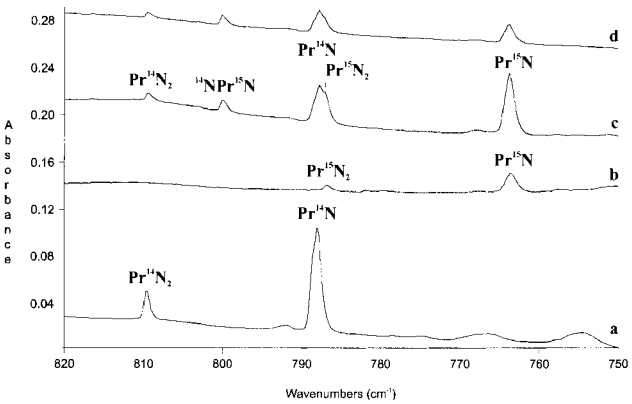

Figure 2. Infrared spectra in the 820−750 cm^{-1} region for laser-ablated praseodymium atoms co-deposited with pure dinitrogen at 6−7 K: (a) $^{14}N_2$ after annealing to 35 K; (b) $^{15}N_2$ after 14 min deposition; (c) mixed N_2 on $^{15}N_2$ after annealing to 32 K; (d) scrambled N_2 after annealing to 32 K.

the energies of cerium nitrides are used to demonstrate the reaction pathways.[28]

$$Ce + N_2 \rightarrow Ce(N_2) \qquad \Delta E = -1.791 \text{ eV} \qquad (5)$$

$$Ce(N_2) + Ce \rightarrow (CeN)_2 \qquad \Delta E = -7.950 \text{ eV} \qquad (6)$$

$$Ce + N_2 \rightarrow CeN + N \qquad \Delta E = +3.303 \text{ eV} \qquad (7)$$

$$Ce + N \rightarrow CeN \qquad \Delta E = -6.815 \text{ eV} \qquad (8)$$

$$2CeN \rightarrow (CeN)_2 \qquad \Delta E = -6.229 \text{ eV} \qquad (9)$$

Experiment favors the first mechanism over the second. Step 7 occurs minimally in argon matrices, as testified by the weak absorption of CeN in argon matrices compared to N_2 films. Given the relative abundance of LnN in nitrogen films, the exothermic step 9 becomes the predominant method of formation, but product bands are weak possibly because of steric hindrance by nitrogen complexation.

$(PrN)_2$. In spectra of argon matrices, both the B_{2u} and B_{3u} modes of this molecule are present. The B_{2u} mode absorbs at 544.9 (528.4) cm^{-1} and exhibits the standard mononitride isotopic nitrogen shift expected for these species and also the regular peak pattern, an isotopic doublet for mixed and a triplet for scrambled experiments. It red-shifts with annealing to 529.3 (513.3) cm^{-1} because of nitrogen complexation of the metal centers. Both peaks with their annealing counterparts are present in mixed-nitrogen experiments, and a central component appears in the scrambled experiments at 535.4 cm^{-1} on deposition and at 520.3 cm^{-1} after the final annealing. The nitrogen film value for this absorption occurs at 531.1 cm^{-1}, in good agreement with the N_2-complexed argon matrix value. In both mixed and scrambled nitrogen films a weak isotopic triplet of peaks is attributed to this vibration.

The B_{3u} mode of $(Pr^{14}N)_2$ absorbs in argon at 670.1 cm^{-1} and shifts with annealing to 639.8 cm^{-1}. The spectra of the B_{3u} mode of $(Pr^{15}N)_2$ are complicated by a Fermi resonance, which provides a doublet for the isolated molecule at 654.5 and 614.5 cm^{-1}. Because of this anomaly, the isotopic ratio for the B_{3u} mode of isolated $(PrN)_2$ is meaningless. After annealing, the B_{3u} mode of NN-complexed $(Pr^{15}N)_2$ absorbs at 621.8 cm^{-1}. Mixed samples show an isotopic doublet, and scrambled samples contain an isotopic triplet with the new central component appearing at 661.9 cm^{-1} before annealing and 630.8 cm^{-1} after annealing. This mode is too weak to be observed in nitrogen films.

$(NdN)_2$. Strong absorptions in argon matrices containing atomic Nd and $^{14}N_2$ ($^{15}N_2$) at 546.7 (530.1) and 679.5 (659.6) cm^{-1} are attributed to the B_{2u} and B_{3u} modes, respectively, of the $(Nd^{14}N)_2$ ($(Nd^{15}N)_2$) molecule. With annealing, the bands shift to 529.4 (513.4) and 657.5 (637.9) cm^{-1}. Mixed-nitrogen samples in argon show an isotopic doublet for each peak, while scrambled samples provide isotopic triplets with central components at 538.2 and 669.6 cm^{-1} before annealing and at 520.5 and 653.0 cm^{-1} after annealing (Figure 5). The experimental isotopic ratios for these peaks are close to the harmonic oscillator ratio for the mononitride. As with the previous metals, both mixed and scrambled nitrogen film experiments yield weak isotopic triplets. This indicates that the formation mechanisms are the same as those modeled previously for the cerium analogue.

$(SmN)_2$. The samarium analogue of the rhombic ring does not absorb as strongly in argon relative to its other lanthanide counterparts. It does, however, show the same characteristic isotopic splitting in argon and in nitrogen matrices as the previous metals. Because the bands are weaker, the complexed molecule cannot be found in argon matrices even after annealing. In mixed and scrambled nitrogen films, the B_{2u} mode of the molecule is too weak to be observed. The experimental nitrogen isotopic shift ratios are compatible with SmN, which is also appropriate for the $(SmN)_2$ molecule.

$(GdN)_2$. Strong bands absorbing at 560.9 (543.6) and 690.2 (669.1) cm^{-1} in the $^{14}N_2$ ($^{15}N_2$) samples with excess argon are assigned, respectively, to the B_{2u} and B_{3u} modes of $(GdN)_2$. The isotopic doublet in mixed-nitrogen samples and isotopic triplet in scrambled nitrogen samples verify that the formation mechanism for this molecule in argon is identical to that of the previous rhombic rings. Annealing causes the peaks to red-shift almost completely to the frequencies found in nitrogen films. Gd deposited into solid N_2 yields an isotopic triplet for each of the two modes in both mixed and scrambled nitrogen films. Comparison of experimental isotopic ratios to harmonic Gd−N ratios supports the assignment.

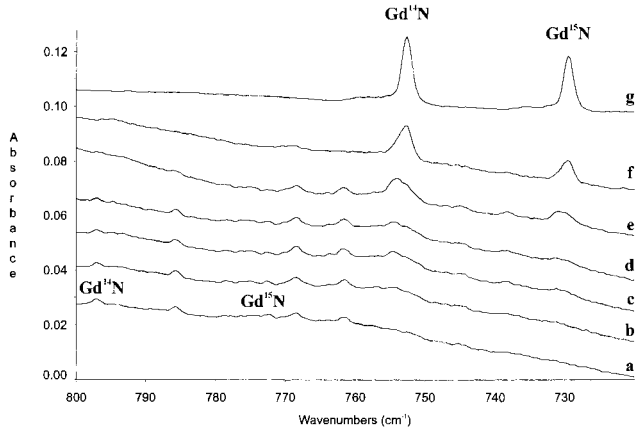

Figure 3. Infrared spectra in the 800−720 cm^{-1} region for laser-ablated gadolinium atoms co-deposited with mixed N_2: (a) 4% in argon after 45 min deposition; (b) 4% in argon after annealing to 27 K; (c) 4% in argon after annealing to 33 K; (d) 4% in argon after 20 min photolysis; (e) 4% in argon after annealing to 39 K; (f) 4% in argon after annealing to 45 K; (g) pure mixed N_2 after 17 min deposition.

Ln_2N. Absorptions found between 450 and 500 cm^{-1} are tentatively assigned to the Ln_2N three-membered ring. This type of molecule was found in argon matrices with the metals Pr, Nd, and Gd and in nitrogen films with Eu. Two isotopic peaks of the observed fundamental are present both in the $^{14}N_2 + {}^{15}N_2$ and the $^{14}N_2 + {}^{14}N^{15}N + {}^{15}N_2$ experiments and provide conclusive evidence that only one N atom is included in the observed vibration (Figure 5). The isotopic frequency ratio is less than the isotopic ratio of the diatomic LnN molecule for praseodymium and neodymium but greater than the LnN ratio for gadolinium and europium, indicating that the angle at the nitrogen atom apex of the three-membered ring is greater than 90° for the former but less than 90° for the latter. A similar absorption observed in the Fe + N_2 system was also assigned to the M_2N ring.[9] The tentative nature of this assignment is accentuated by the possibility of intermediate peaks in the scrambled oxygen sample, dwarfed by the primary pure isotopic absorptions (Figure 5). Site splitting in the pure isotopic spectra both above and below the primary absorptions precludes a definitive assignment of this weak structure to either additional isotopic absorptions or matrix splitting.

Dinitrogen Complexes. There are two basic orientations of dinitrogen with respect to a complexed Ln metal center: end-bound (η^1-N_2) or (NN); side-bound (η^2-N_2) or (N_2). Commonly identifiable complexes include Ln(NN), $Ln(NN)_2$, $Ln(NN)_x$, the coordinatively saturated metal center (Figure 1), and $Ln(N_2)$ (Figure 6). The $Ln(NN)_2$ and $Ln(N_2)$ species exhibit nearly coincident absorptions in the mid-1700 cm^{-1} region (Figure 6). The fully coordinated metal center, presumably with end-bound dinitrogens, absorbs near 2100 cm^{-1}. In addition, the ionic complex $Ln^+(N_2)_2^-$ is tentatively assigned about 200 cm^{-1} lower than the $Ln(N_2)$ and $Ln(NN)_2$ complexes. Other peaks present in this region of the spectrum may be attributed to various intermediate N_2 complexes of one or both of the above types but with an indeterminate number of ligands. Complexes that can be correlated with nitride product molecules are also identified.

Ln(NN). The Ln(NN) complex is observed in argon for Ce and Gd and in nitrogen for Sm between 1550 and 1580 cm^{-1}. It is characterized by a pure dinitrogen isotopic ratio and mixed isotopic doublet and scrambled isotopic triplet of peaks, indicating a single N_2 subunit. This peak increases with annealing as metal atoms in the matrix associate with dinitrogen ligands.

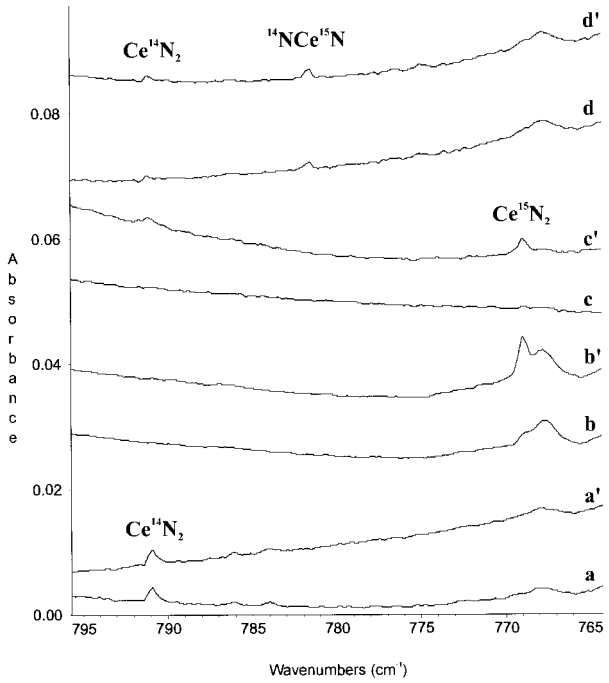

Figure 4. Infrared spectra in the 795−765 cm^{-1} region for laser-ablated cerium atoms co-deposited with 2% N_2 in argon: (a) $^{14}N_2$ before photolysis; (a′) $^{14}N_2$ after photolysis; (b) $^{15}N_2$ before photolysis; (b′) $^{15}N_2$ after photolysis; (c) $^{14}N_2 + {}^{15}N_2$ before photolysis; (c′) $^{14}N_2 + {}^{15}N_2$ after photolysis; (d) $^{14}N_2 + {}^{14}N^{15}N + {}^{15}N_2$ before photolysis; (d′) $^{14}N_2 + {}^{14}N^{15}N + {}^{15}N_2$ after photolysis.

$Ln(NN)_2$. In argon, the NN antisymmetric vibration of this complex is observed between 1770 and 1740 cm^{-1} for all of the lanthanides studied except Eu; all six exhibit this complex in nitrogen. The $^{14}N/^{15}N$ ratio for this complex clearly indicates an NN motion in all cases. Furthermore, the mechanically mixed samples show a triplet of peaks, and the scrambled samples show a higher multiplet, indicative of the motion of two dinitrogen units (traces g and h of Figure 6). Because the N atoms are symmetry-inequivalent within each dinitrogen unit, the isotopically scrambled samples should exhibit decet splitting. Like $Th(NN)_2$, coalescence of several of these isotopic splittings yields sextet splitting in a 1:4:4:2:4:1 proportion rather than the expected decet.[29] In mixed samples, the isotopic triplet for the antisymmetric vibration is supplemented by the ($^{14}N^{14}N$)Ln($^{15}N^{15}N$) sym-metric vibration found as a weaker broad peak higher than the triplet.

In nitrogen films, the overtone for the antisymmetric stretch of these molecules can be seen in the 3500 cm^{-1} region (Figure 6). Although the mixed and scrambled isotopic components of the overtone have never absorbed strongly enough to be determined, the overtone is consistently observed for the $^{14}N_2$ and $^{15}N_2$ films and tracks with the fundamental. In most cases, there is no other peak present in the mid-1700 cm^{-1} region that could be the fundamental of the 3500 cm^{-1} overtone. For Sm-$(NN)_2$ and Eu$(NN)_2$, the two cases where another peak is present with an overtone in the same region, behavior on annealing and photolysis distinguishes the overtones from each other. The overtone of $Ln(NN)_2$ exceeds twice the value of the fundamental by 20−30 cm^{-1}, demonstrating positive anharmonicity. Because the complex is linear, normally insignificant quartic terms become important in the anharmonicity and in this case lead to positive rather than negative anharmonicity.

$Ln(NN)_x$. The fully coordinated metal center is found for all metals in nitrogen and after annealing in argon matrices near

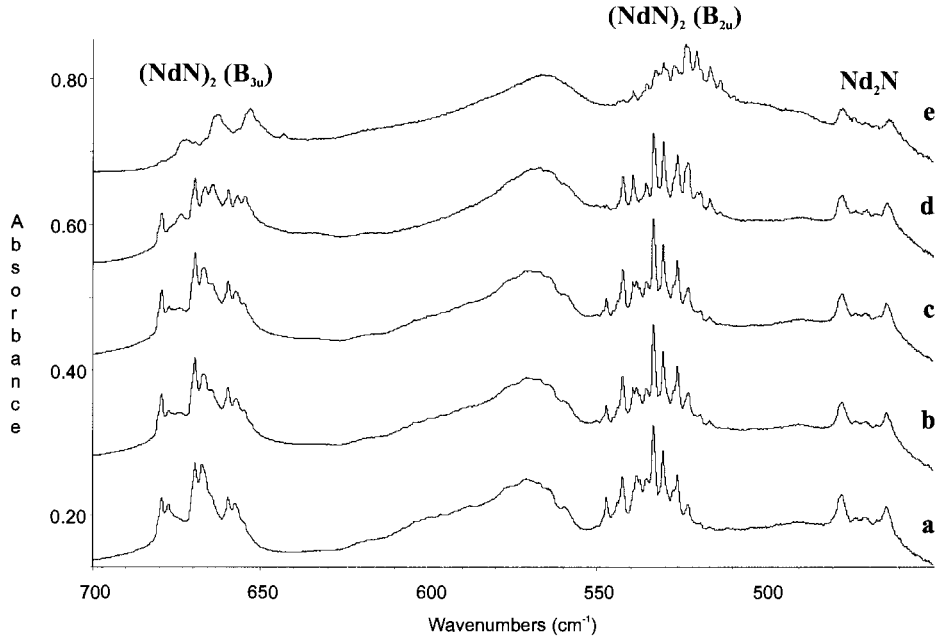

Figure 5. Infrared spectra in the 700−450 cm^{-1} region for laser-ablated neodymium atoms co-deposited with 2% $^{14}N_2 + {}^{14}N^{15}N + {}^{15}N_2$ in argon: (a) after 1 h deposition at 6−7 K; (b) after annealing to 28 K; (c) after 15 min photolysis; (d) after annealing to 35 K; (e) after annealing to 42 K.

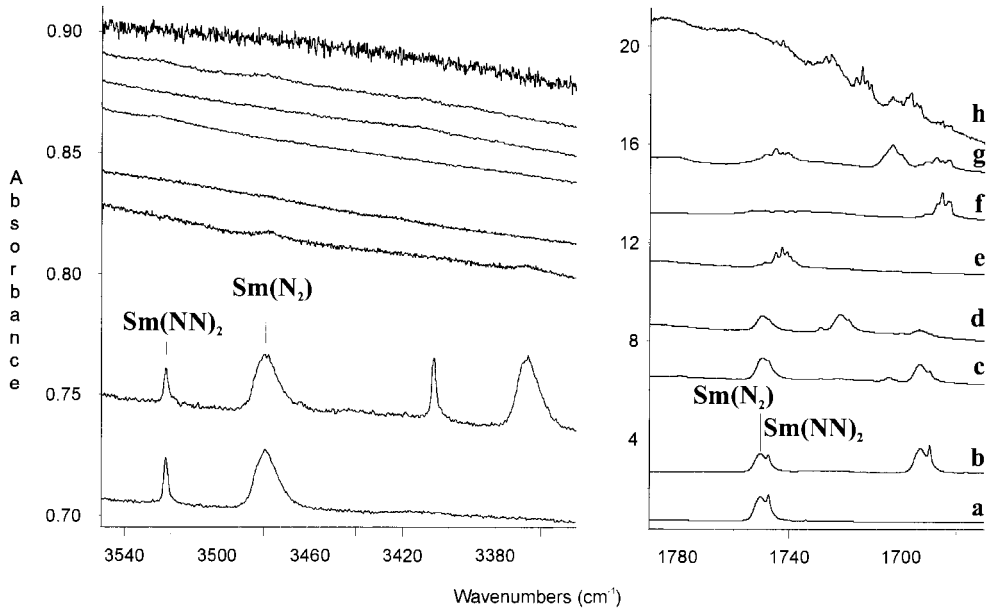

Figure 6. Infrared spectra in the 3550−3345 and 1790−1670 cm^{-1} regions for laser-ablated samarium atoms co-deposited with pure nitrogen: (a) after 20 min deposition with $^{14}N_2$ at 6−7 K; (b) after 20 min deposition with $^{15}N_2$ on $^{14}N_2$ at 6−7 K; (c) after 20 min deposition with $^{14}N_2 + {}^{15}N_2$ at 6−7 K; (d) after 20 min deposition with $^{14}N_2 + {}^{14}N^{15}N + {}^{15}N_2$ at 6−7 K, with 2% N_2 in argon; (e) $^{14}N_2$ after annealing to 28 Kl (f) $^{15}N_2$ after annealing to 28 K; (g) $^{14}N_2 + {}^{15}N_2$ after annealing to 28 K; (h) $^{14}N_2 + {}^{14}N^{15}N + {}^{15}N_2$ after annealing to 28 K.

2100 cm^{-1} (Figure 1). It is the dominant peak in nitrogen films and becomes dominant in argon after the conclusion of annealing cycles, yielding a very broad doublet with mechanically mixed nitrogen and a triplet with scrambled nitrogen samples. The mixed doublet also shows some smaller intensity between the two peaks, which can be attributed to various combinations of $^{14}N_2$ and $^{15}N_2$ interactions across the metal center.

Ln(N$_2$). This complex absorbs near 1750 cm^{-1} and has been identified for the samarium and europium systems in argon matrices and nitrogen films. These bands are assigned on the basis of the doublet seen in mechanically mixed samples and the isotopic triplet in scrambled samples, which evidence together indicates the presence of exactly one dinitrogen unit with symmetry-equivalent N atoms. In addition, in solid nitrogen, overtone bands are seen in the 3400 cm^{-1} region, identified in Tables 4 and 5 and demonstrated for samarium in Figure 6.

Ln$^+$(N$_2$)$_2^-$. The dinitrogen frequencies for these complexes (Ln = Ce, Pr, Nd, Gd) are found in the 1500−1600 cm^{-1} region. Nitrogen isotopic splittings show a 1:2:1 triplet of peaks for mechanically mixed samples and a sextet of peaks in a 1:4:4:2:4:1 proportion for scrambled samples, indicating that two dinitrogen units are involved in this mode. The $^{14}N/^{15}N$ peak ratios for these complexes in argon are unusually low for NN modes, as can be seen in Tables 1−3. Because it is known that low-lying electronic states exist on lanthanide metal atoms, it is postulated that vibronic coupling of the observed NN stretches with a low-lying Ln electronic state alters the frequency

of one of the isotopic absorptions, lowering the $^{14}N/^{15}N$ ratios.[30] When found in nitrogen films, the $^{14}N/^{15}N$ ratios are normal for NN vibrational modes. Ce, Pr, and Nd, the metals for which this complex was identified under both matrix conditions, show an argon value in excess of the nitrogen film value. This discrepancy is likely all that is necessary to uncouple the electronic and vibrational states. This peak decreases with photolysis, consistent with an anionic species.

$(NN)_x(LnN)_2(NN)_x$. Since it is obvious from the data presented in Tables 1−6 that the rhombic ring nitrides complex dinitrogen, an effort was made to assign the N−N absorption due to this complexation. Comparison of annealing spectra of argon matrices containing the rhombic ring nitrides allowed identification of a broad band consistently located between 2320 and 2300 cm^{-1}, shown in Tables 1−6, that tracks well with the ring absorptions. This band is postulated to be due to the N−N absorptions of the $(NN)_x(LnN)_2(NN)_x$ complexes.

Conclusions

For the first time the infrared spectra of the simple nitrides and dinitrogen complexes of the first six lanthanide metals in solid argon and in nitrogen have been reported. The three commonly found nitrides are of the type LnN, LnN_2, and $(LnN)_2$. Different mechanisms of formation of the LnN_2 and $(LnN)_2$ molecules are found to prevail depending on the composition of the matrix. Cerium is observed to insert into the N_2 bond with UV photolysis of the matrix. Side-on bonding of the N_2 ligand to either one or two lanthanide metals appears to be instrumental in the activation of dinitrogen prior to subsequent formation of nitride molecules.

$Ln(N_2)$ is an important intermediate in the formation of both $(LnN)_2$ and LnN_2. Thermodynamic calculations confirm experimental evidence that the $Ln(N_2)$ intermediate is much more likely to bind an additional Ln atom forming $(LnN)_2$ and releasing about 8 eV than it is to insert, forming LnN_2 and releasing about 0.03 eV, although the latter reaction is facilitated by UV photons.[28]

Acknowledgment. We gratefully acknowledge financial support from the National Science Foundation, Grant CHE 97-00116.

References and Notes

(1) Gingerich, Karl A. *J. Chem. Phys.* **1971**, *54*, 3720.
(2) Douglas, A. E.; Veillette, P. J. *J. Chem Phys.* **1980**, *72*, 5378.
(3) Berezin, A. B.; Dmitvuk, S. A.; Kataev, D. I. *Opt. Spectrosc. (USSR)* **1990**, *68*, 310.
(4) Ram, R. S.; Bernath, P. F.; Balfour, W. J.; Cao, J.; Qian, C. X. W.; Rixon, S. J. *J. Mol. Spec.* **1994**, *168*, 350.
(5) Kushto, G. P.; Souter, P. F.; Andrews, L. To be submitted.
(6) Andrews, L.; Souter, P. S.; Bare, W. D. To be published.
(7) Zhou, M.; Andrews, L. *J. Phys. Chem. A* **1998**, *102*, 9061.
(8) Bates, J. K.; Gruen, D. M. *J. Chem. Phys.* **1979**, *70*, 4428.
(9) Chertihin, G. V.; Andrews, L.; Neurock, M. *J. Phys. Chem.* **1996**, *100*, 14609.
(10) Andrews, L.; Bare, W. D.; Chertihin, G. V. *J. Phys. Chem. A* **1997**, *101*, 8417.
(11) Andrews, L.; Citra, A.; Chertihin, G. V.; Bare, W. D.; Neurock, M. *J. Phys. Chem.* **1998**, *102*, 2561.
(12) Chertihin, G. V.; Andrews, L.; Bauschlicher, C. W., Jr. *J. Am. Chem. Soc.* **1998**, *120*, 3205.
(13) Andrews, L. *J. Electron Spectrosc. Related Phenom.*, in press.
(14) Chertihin, G. V.; Bare, W. D.; Andrews, L. *J. Phys. Chem. A* **1998**, *102*, 3697.
(15) Dolg, M.; Stoll, H. *Theor. Chim. Acta* **1989**, *75*, 369.
(16) Wang, S. G.; Schwarz, W. H. E. *J. Phys. Chem.* **1995**, *99*, 11687.
(17) Wang, S. G.; Pan, D. K.; Schwarz, W. H. E. *J. Chem. Phys.* **1995**, *102*, 9296.
(18) Lesar, A.; Muri, G.; Hodoscek, M. *J. Phys. Chem.* **1998**, *102*, 1170.
(19) Evans, W. J.; Ulibarri, T. A.; Ziller, J. W. *J. Am. Chem. Soc.* **1988**, *110*, 6877.
(20) Desmangles, N.; Jenkins, H.; Ruppa, K. B.; Gambarotta, S. *Inorg. Chim. Acta* **1996**, *250*, 1.
(21) Lee, D. W.; Kaska, W. C.; Jensen, C. M. *Organometallics* **1998**, *17*, 1.
(22) Burkholder, T. R.; Andrews, L. *J. Chem. Phys.* **1991**, *95*, 8697.
(23) Hassanzadeh, P.; Andrews, L. *J. Phys. Chem.* **1992**, *96*, 9177.
(24) Tian, R.; Facelli, J. C.; Michl, J. *J. Phys. Chem.* **1988**, *92*, 4073.
(25) Willson, S. P.; Andrews, L. To be submitted.
(26) DeKock, R. L.; Weltner, W, Jr. *J. Phys. Chem.* **1971**, *75*, 514.
(27) Gabelnick, S. D.; Reedy, G. T.; Chasanov, M. G. *J. Chem. Phys.* **1974**, *60*, 1167.
(28) *ADF 2.1, Theoretical Chemistry*; Vrije Universiteit: Amsterdam (triple-ζ basis sets, 5d frozen cores).
(29) Kushto, G. P.; Souter, P. F.; Andrews, L. *J. Chem. Phys.* **1998**, *108*, 7121.
(30) Martin, W. C., Zalubas, R., Hagan, L., Eds. *Atomic Energy Levels—The Rare-Earth Elements*; U.S. Department of Commerce, National Bureau of Standards: Washington, DC, 1978.